Interband critical points of GaAs and their temperature dependence

P. Lautenschlager, M. Garriga, S. Logothetidis,* and M. Cardona
Max-Planck-Institut für Festkörperforschung, Heisenbergstrasse 1, Postfach 80 06 65, D-7000 Stuttgart 80, Federal Republic of Germany
(Received 10 October 1986)

The complex dielectric function $\epsilon(\omega)$ of GaAs was measured from 20 to 750 K with a scanning rotating-analyzer ellipsometer. The structures observed in the 1.3—5.5-eV photon-energy region, attributed to transitions near the Γ point of the Brillouin zone (E_0, $E_0+\Delta_0$, E_0'), along the Λ direction (E_1, $E_1+\Delta_1$), and near the X point (E_2), are analyzed by fitting the second-derivative spectrum $d^2\epsilon(\omega)/d\omega^2$ to analytic critical-point line shapes. The E_0' and E_2 critical points are best fitted in the whole temperature region by a two-dimensional line shape, whereas the E_1 and $E_1+\Delta_1$ transitions are best fitted up to room temperature by a Lorentzian interacting with a continuum of interband transitions (Fano line shape). The excitonic character of the E_1 and $E_1+\Delta_1$ transitions is discussed within several theoretical approaches. The experiments indicate that up to room temperature the localized Lorentzian interacting with the continuum is dominant, whereas at higher temperatures the modification of the two-dimensional Van Hove singularity due to the electron-hole attractive perturbation is a better description of the measurements. For all critical points, the energy decreases with increasing temperature while the broadening increases. This dependence on temperature is analyzed in terms of averaged phonon frequencies which cause a renormalization of the energies and a broadening of the band gaps.

I. INTRODUCTION

GaAs is a material of great physical interest and technological importance. Because of the small effective mass it can yield high electron mobility and thus be used as a model semiconductor for high-speed electronic devices. It can also be considered as a prototype of a direct-band-gap material, germanium and silicon having an indirect gap. Because of this, the emission of light is very effective in GaAs and the material is ideal for opto-electronic applications. In addition, due to the nearly perfect lattice match of GaAs to AlAs it is possible to grow heterostructures from GaAs, AlAs, and the mixed crystal $Al_xGa_{1-x}As$ in order to create artificial materials with tailored electronic and optical properties. The small effective electron mass also results in strong optical confinement effects in these superlattices.

Many applications of GaAs depend on the dielectric function $\epsilon(\omega)$. This function is related to the electronic band structure and can be used as a powerful source of experimental information on the latter. It has been shown that spectroscopic ellipsometry is highly suitable to determine the dielectric function of semiconductors.[1] Silicon, germanium, and many III-V compounds have been investigated by this method in the 1.5—6-eV photon-energy region.[1] The structures observed in the $\epsilon(\omega)$ spectra are attributed to interband critical points (CP's) which can be analyzed in terms of standard analytic line shapes:[2,3]

$$\epsilon(\omega)=C-Ae^{i\phi}(\omega-E+i\Gamma)^n . \quad (1)$$

The critical-point parameters amplitude A, energy threshold E, broadening Γ, and excitonic phase angle ϕ are determined by fitting the numerically obtained second-derivative spectra $d^2\epsilon(\omega)/d\omega^2$ of the experimental $\epsilon(\omega)$. (The exponent n has the value $-\frac{1}{2}$ for one-dimensional (1D), 0 [logarithmic, i.e., $\ln(\omega-E+i\Gamma)$] for 2D, and $\frac{1}{2}$ for 3D CP's. Discrete excitons with Lorentzian line shape are represented by $n=-1$). From the fact that CP's are directly related to regions of large or singular joint electronic density of states direct information on the energy separation of valence and conduction bands (interband gaps) is obtained, which can be compared with band-structure calculations.

The band structure of GaAs, as calculated by Chelikowsky and Cohen,[4] is shown in Fig. 1. Several interband

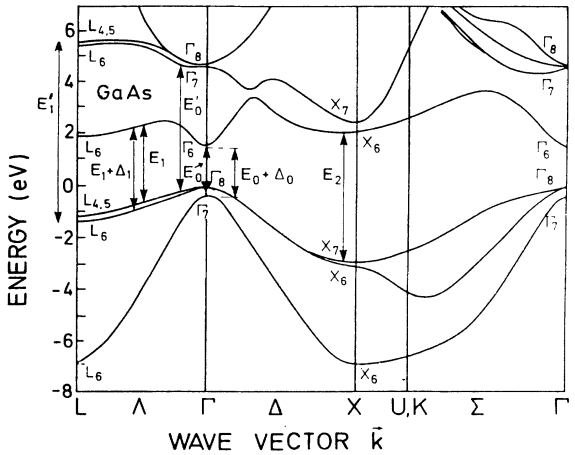

FIG. 1. Band structure of GaAs reproduced from Ref. 4 showing the main interband critical points.

transitions are indicated. The fundamental absorption edge of GaAs (E_0) is dominated by the free exciton, a fact which is particularly evident at low temperatures.[5] Its energy is 4.2 meV less than the lowest direct band gap E_0 (Ref. 6) which is located at the Γ point of the Brillouin zone (BZ). The second lowest interband critical point, $E_0+\Delta_0$, corresponds to transitions from the larger component of the spin-orbit-split valence band to the lowest conduction band at the Γ point. The next higher interband transitions are labeled E_1 and $E_1+\Delta_1$. They take place along the Λ lines of the BZ ($\langle 111 \rangle$ directions). In the energy region from 4 to 5.5 eV several CP's have been resolved.[7] The most prominent ones have been assigned to transitions near the Γ point (E_0' with their spin-orbit-split counterparts) and at several points or extended regions near the X point (E_2 CP's).

Measurements of these interband transitions in GaAs have been performed by several optical techniques, such as photoluminescence[8,9] (for the E_0 transitions), absorption,[5,10–13] Faraday rotation,[14] resonant Raman scattering,[15] reflectance,[11,16–22] and several reflectance-modulation techniques such as piezoreflectance,[23,24] magnetoreflectance,[25] thermoreflectance,[26–28] electroreflectance[7,29–37] and wavelength-modulated reflectance.[38–40] Some authors have systematically investigated the temperature dependence of the gap energies. The E_0 gap was studied by absorption,[5] reflectivity,[41] electroreflectance,[29] and piezoreflectivity[24] from low temperatures to room temperature. Absorption measurements have been performed up to 1000 K.[10] The temperature dependence of transitions above the fundamental gap has been measured in the temperature range below 300 K by absorption,[13] reflectance,[20] wavelength-modulation reflectance,[39] thermoreflectance,[27] and electroreflectance.[29] Many band-structure calculations have been performed with various semiempirical methods,[4,42–44] and also with first principles ("*ab initio*") techniques.[45] Also, the effect of spin-orbit splitting on the band structure has been studied in some detail.[46,47]

The temperature dependence of important critical points in the band structure has been calculated taking into account the thermal expansion and the electron-phonon interaction. The latter was included by softening the pseudopotential form factors with temperature-dependent Debye-Waller factors.[23,40,48–50] However, it has been shown[51–53] that a second contribution to the electron-phonon interaction, arising from the so-called Fan[54,55] or "self-energy" terms, is of the same order of magnitude as the Debye-Waller terms and should be included in the calculations. This is rather cumbersome and has, so far, been only done for germanium, silicon, and the E_0 gap of GaAs.

In the past few years our group has been engaged in the systematic investigation of the dependence of the critical-point parameters on temperature,[56–60] concentration of donors and acceptors,[61,62] and composition in mixed crystals.[63,64] In parallel with this experimental work, calculations of the shift and broadening with donor and acceptor concentration[61,62] and temperature[65–69] have been performed, the latter including the Fan or self-energy contribution to the electron-phonon interaction.

In this paper we investigate the temperature dependence of the optical constants and the critical-point parameters of undoped GaAs for temperatures from 20 to 750 K in the photon-energy range from 1.3 to 5.6 eV. We present data for the E_0, $E_0+\Delta_0$, E_1, $E_1+\Delta_1$ and the transitions in the uv region, mainly E_0' and E_2. In Sec. II we describe the experimental setup, in Sec. III we present the results of our analysis of the several interband transitions. Generally, we observe, as in other group-IV elemental and III-V compound[56–58] semiconductors, a decrease of the CP energies with temperature and an increase of the broadening parameters. We also observe a decrease of the excitonic phase angle ϕ [Eq. (1)], indicating that excitonic interaction decreases with increasing temperature. The temperature dependence of the CP energies and broadening can usually be described by empirical relations like Varshni's equation[70] and also by a more microscopic expression which contains an average Bose-Einstein statistical factor for the phonons.[56,71] In some cases, however, linear fits are performed. The Varshni and Bose-Einstein relations contain a parameter which is connected to an average phonon frequency of the phonons which contribute to shift and broadening of the gaps via electron-phonon interaction.

Special attention is paid to the character of the E_1 and $E_1+\Delta_1$ transitions. The description of Coulomb interaction (excitonic effects) by a phase factor $e^{i\phi}$ in Eq. (1), which allows a mixture of two adjacent CP's, holds if the band or continuum character is dominant. If a localized excitation interacts with a continuum, the line shape is described by the Fano-Breit-Wigner profile.[72,73] In the case of the E_1 and $E_1+\Delta_1$ transitions we find that up to room temperature the latter gives a better representation of the experimental second-derivative spectra of $\epsilon(\omega)$. In Sec. IV we discuss our results on the temperature dependence of the CP parameters and the character of the transitions, including an attempt to describe the excitonic effect with the Koster-Slater contact interaction.[2]

II. EXPERIMENTAL

The measurements were performed on a sample cut from a n-type GaAs ingot with $n<10^{16}$ cm^{-3} [at room temperature (RT)] and a [100] surface orientation. Before mounting the sample into the cryostat, a wet-chemical etching was carried out to obtain the largest dielectric discontinuity between sample and ambient by removing surface overlayers. This can be conveniently done by maximizing the value of $\epsilon_2(\omega)$ in the E_2 region which is most sensitive to the presence of overlayers.[1,74] We optimized ϵ_2 at E_2 by rinsing the sample with H_2O followed by an etch with a solution of 0.05 vol% bromine in methanol and a 1:1 solution of NH_4OH in H_2O.[1] Real-time ellipsometric measurements at the energy of 4.8 eV ($\sim E_2$) were taken while performing the etching. The treatment was repeated until the largest stable value of ϵ_2 [ϵ_2 (4.8 eV)=22.7] was obtained. During the etching procedure the sample was kept at room temperature in a windowless glass cell in flowing dry N_2 so as to minimize surface contamination. After etching, the sample was placed in the cryostat which was closed also in a N_2 atmosphere.

The cryostat consists of a stainless-steel chamber with high-quality stress-free fused quartz windows[56] evacuated with a turbo-molecular pump. After baking out the system at ~160 °C the vacuum was better than 2×10^{-8} Torr (at RT) which is necessary to avoid condensations at low temperatures.[56,75] Two different cold-finger-type sample holders were used, one for cooling with liquid He, where the sample was glued with silver paint ("Leitsilber").[76] The other sample holder can be cooled by liquid N_2 and has a heating system built into the cold finger so as to raise the temperature from 85 K up to 800 K. Here the sample was held against the sample holder by two copper strips at the top and the bottom and a commercial cement[77] at the backside to get good thermal contact with the holder. The sample temperature was determined with three appropriately calibrated iron-constantan thermocouples placed above, below, and onto the sample, the latter with the aid of one of the copper strips. The temperature stability was typically ±3 K up to 80 K and ±1 K at higher temperatures. During the low-temperature measurements the vacuum was better than 10^{-8} Torr, slightly worsening at higher temperatures.

The measurements were performed with an automatic spectral ellipsometer of rotating analyzer type[78] with the same optical setup as described in Ref. 56. The energy spacing of the experimental points was 10 meV in the photon-energy region from 1.7 to 5.6 eV. In the region of the edge exciton we used a 0.5-meV mesh at low temperatures (spectral slit width ~0.6 meV) and a 2-meV mesh from 150 K to higher temperatures. All the spectra were taken at an angle of incidence of 67.5°. The calibration procedure for the system[79] was carried out at each temperature to correct for possible changes of the sample position due to the thermal expansion of the sample holder.

III. RESULTS

Ellipsometry measures the complex ratio ρ of the reflection coefficients r_P and r_S ($\rho=r_P/r_S\equiv\tan\psi e^{i\Delta}$). If there is no overlayer present, the dielectric function $\epsilon(\omega)=\epsilon_1(\omega)+\epsilon_2(\omega)$ is calculated with the two-phase model:[80] ambient (air or vacuum) crystal. In our case, due to the transfer of the sample to the cryostat and the process of outgassing, an oxide layer was still present as indicated by the decrease of the value of ϵ_2 at E_2, calculated in the two-phase model, from ϵ_2 (4.8 eV)=22.7 after the etching to ϵ_2 (4.8 eV)=18.1 after baking out the cryostat. Within a three-phase model (air-oxide of GaAs—bulk GaAs), and with data for the dielectric function of the oxide taken from the literature,[81] we calculated the film thickness to be 11 Å by forcing the value of ϵ_2 (4.8 eV) of the sample to become again 22.7. The calculations within the three-phase model were performed numerically by solving the equations for the complex reflectance ratio using the two-dimensional Newton's method.[82]

Aspnes and Studna[1] obtained a value of ϵ_2 (4.8 eV)=25.2. From our data, we obtain this value for the GaAs substrate by assuming a 16.4-Å-thick oxide overlayer. For comparison, we show in Fig. 2 our data obtained at room temperature with the sample mounted in the cryostat and after a correction for an oxide layer of 16.4 Å within the three-phase model, together with the data of Ref. 1 obtained directly after wet-chemical processing techniques.

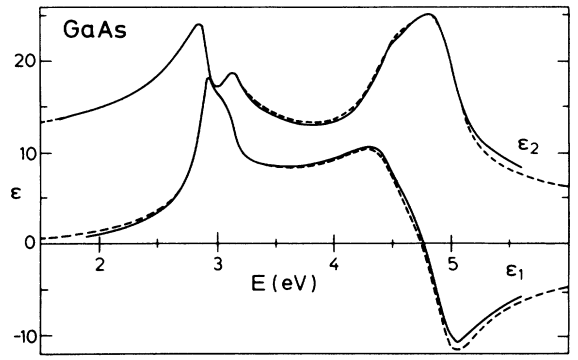

FIG. 2. Solid line, real (ϵ_1) and imaginary (ϵ_2) part of the dielectric function of GaAs measured at room temperature with the sample inside our cryostat. Dashed line, data obtained after wet-chemical processing (Ref. 1).

In Figs. 3 and 4 we show the real and imaginary parts of the dielectric function of the GaAs substrate for several temperatures after correction for a 16.4-Å oxide layer. We assumed that the dielectric function of the layer is independent of temperature. The main structures are due to the E_1, $E_1+\Delta_1$, E_0', and E_2 transitions which are clearly observed from 22 K up to 750 K. Other weak transitions, such as E_0, $E_0+\Delta_0$, and some others in the 4.2—5.5 eV photon-energy region, are observed only at lower temperatures and are partly difficult to distinguish in these figures.

In order to enhance the structure present in the spectra and to obtain the CP parameters, we calculate numerically the second-derivative spectra, $d^2\epsilon/d\omega^2$, of the complex dielectric function from our ϵ data. Tabulated coefficients for fitting a polynomial of degree five to the experimental data and performing directly the second derivative have been taken from the literature.[83] By taking into account an appropriate number of points the derivative spectra can be smoothed out without substantially distorting the line shape.

Figure 5 shows the experimental second-derivative spectrum of ϵ_1 at 22 K in the spectral regions where struc-

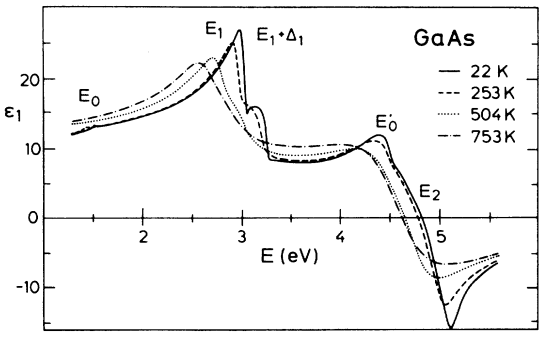

FIG. 3. Real part of the dielectric function of GaAs for several temperatures.

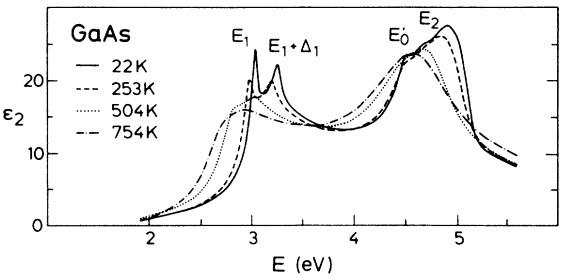

FIG. 4. Imaginary part of the dielectric function of GaAs for several temperatures.

tures are observed. The lines represent the best fits to standard critical-point line shapes, derived from Eq. (1):

$$\frac{d^2\epsilon}{d\omega^2}=\begin{cases}-n(n-1)Ae^{i\phi}(\omega-E+i\Gamma)^{n-2}, & n\neq 0\ , \quad (2a)\\ Ae^{i\phi}(\omega-E+i\Gamma)^{-2}, & n=0\ . \quad (2b)\end{cases}$$

For the fit we use a least-square procedure where both real and imaginary parts of $d^2\epsilon/d\omega^2$ are fitted simultaneously.

If the angle ϕ in the phase factor $e^{i\phi}$ in Eqs. (1) and (2) takes values which are integer multiples of $\pi/2$, the line shape corresponds to transitions between uncorrelated one-electron bands while noninteger multiples represent the inclusion of excitonic effects by allowing a mixture of two CP's.[2,84,85] In Eq. (1), taking $A>0$ and $n=\frac{1}{2}$ for a 3D CP, $\phi=0$, $\pi/2$, π, and $3\pi/2$ correspond to M_1, M_2, M_3, and M_0 CP's, respectively. By taking $A>0$ and $n=0$ for a 2D CP, $\phi=0$, $\pi/2$, and π correspond to a minimum, saddle point, and maximum, respectively. For a discrete excitonic line shape ($n=-1$) a phase angle of $\phi\neq 0$ corresponds to a Fano-profile, i.e., the line shape which results from the interaction of the discrete excitation with a continuous background, as discussed below.

We have fitted the E_0 and $E_0+\Delta_0$ structures with excitonic line shapes [$n=-1$ in Eq. (2)]. Because of the poor accuracy of the values of ϵ_2 for small ϵ_2 in rotating analyzer ellipsometers without compensator,[1,86] we have analyzed these structures only in the real part of the dielectric function. In the case of the E_1 and $E_1+\Delta_1$ CP's both ϵ_1 and ϵ_2 were fitted. The best fits were obtained with an excitonic line shape from the lowest temperatures up to room temperature, whereas at higher temperatures a 2D line shape [$n=0$ in Eq. (2)] yielded the best representation of the experimental data. At every temperature E_1 and $E_1+\Delta_1$ were fitted simultaneously with the same phase angle ϕ for both CP's and a fixed spin-orbit splitting of $\Delta_1=224$ meV, which was obtained from the spectra at low temperatures. The two structures in the near-uv region, E_0' and E_2, were also fitted simultaneously with two 2D line shapes, which gave the best fits over the whole temperature range. For the fit of the three weak structures in between [labeled $E_0'+\Delta_0'$ and $E_2(\Sigma)$ in Fig. 5] a 2D line shape was used as well.

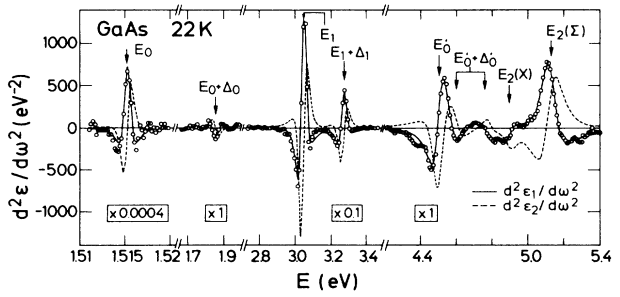

FIG. 5. Fits to the second derivatives of the real (solid line) and imaginary (dashed line) parts of the dielectric function of GaAs as a function of energy at 22 K. When reading from the vertical scale, the value has to be divided by the factor, given in the box under each structure. Note the change in the energy scale for the E_0 transition.

In Fig. 6 we show the CP energies obtained from our line-shape analysis for the main transitions observed in GaAs as a function of temperature. In spite of the change of the line shape of the E_1 and $E_1+\Delta_1$ transitions from excitonic to 2D at RT, the data for the CP energy match smoothly in both regions. The energies of the $E_1+\Delta_1$, CP's are not shown, they run parallel to E_1, displaced by 224 meV. At low temperatures the gaps depend quadratically on temperature and linearly at higher temperatures. This behavior can be described by two equations: Varshni's empirical relation[70]

$$E(T)=E(0)-\frac{\alpha T^2}{T+\beta}\ , \quad (3a)$$

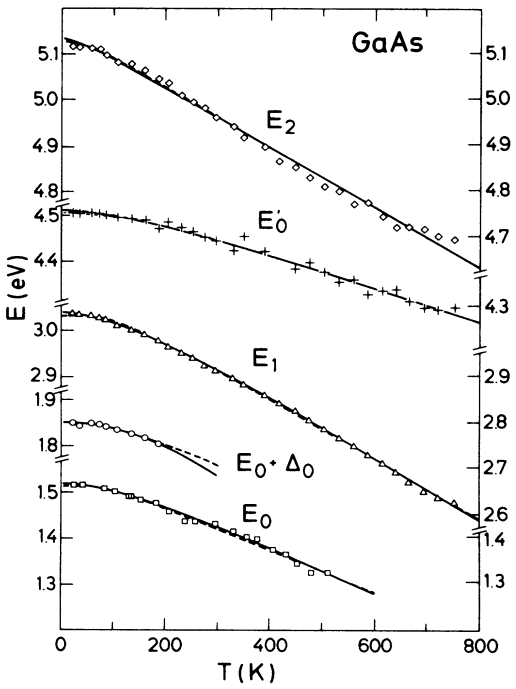

FIG. 6. Temperature dependence of the interband critical-point energies of GaAs. The solid lines represent the best fits with Eq. (3a); the dashed lines correspond to the fit with Eq. (3b). Typical error bars for the experimental points are given in Table III, the fit parameters in Table I.

TABLE I. Values of the parameters $E(0)$, α and β obtained by fitting the critical-point energies versus temperature to the equations $E(T)=E(0)-\alpha T^2/(T+\beta)$, and values of E_B, a_B, and Θ obtained by fitting with the equation $E(T)=E_B-a_B[1+2/(e^{\Theta/T}-1)]$. The numbers in parentheses indicate error margins.

	$E(0)$ (eV)	α (10^{-4} eV K^{-1})	β (K)	E_B (eV)	a_B (meV)	Θ (K)	Line shape
E_0	1.517(8)	5.5(1.3)	225(174)	1.571(23)	57(29)	240(102)	Excitonic
$E_0+\Delta_0$	1.851(5)	3.5(4)	225(fixed)	1.907(9)	58(7)	240(fixed)	Excitonic
E_1	3.041(3)	7.2(2)	205(31)	3.125(9)	91(11)	274(30)	Excitonic (−300 K) 2D (300–760 K)
E_0'	4.509(8)	4.0(7)	241(177)	4.563(21)	59(26)	323(119)	2D
E_2	5.133(21)	6.6(4)	43(66)	5.161(33)	38(33)	114(95)	2D

and an average Bose-Einstein statistical factor for phonons with an average frequence Θ,[56,57]

$$E(T)=E_B-a_B\left[1+\frac{2}{e^{\Theta/T}-1}\right]. \tag{3b}$$

The values of the parameters obtained through fits with Eqs. (3a) and (3b) are given in Table I for the transitions shown in Fig. 6 with the corresponding uncertainties representing 95% reliability. The temperature dependence of the Lorentzian broadening parameters Γ for E_1 and $E_1+\Delta_1$ CP's are shown in Fig. 7(a) for the fit of these structures with an excitonic line shape up to 550 K and with a 2D CP over the whole temperature range. Fits to the broadening versus temperature have been performed only in the temperature range where the corresponding line shape yields the best fit to the experimental second-derivative spectra, i.e., for 22–300 K for the data from the fit to the excitonic line shape and for 300–760 K for the 2D one. The discontinuity in Γ near 300 K is due to the fact that the absolute values of the broadenings depend on the dimensionality of the CP chosen for the fit.[56] The temperature dependence of the broadening has been described by a formula similar to Eq. (3b):[56,68]

$$\Gamma(T)=\Gamma_0\left[1+\frac{2}{e^{\Theta/T}-1}\right]+\Gamma_1. \tag{4}$$

When fitting our data in the 20–300 K temperature range for E_1 and $E_1+\Delta_1$ we found that the inclusion of the third parameter Γ_1 does not significantly improve the representation of the data. A linear equation

$$\Gamma(T)=\Gamma_L+\gamma T \tag{5}$$

was used to describe the temperature dependence of the broadenings obtained from the 2D fit in the 300–760 K range. The fitted parameters with their corresponding uncertainties are listed in Table II.

In the inset of Fig. 7(a), the Γ's obtained for the E_0 transition are shown up to 300 K, fitted with Eq. (4). In Fig. 7(b) the broadening parameters for the E_0' and E_2 CP's are shown, the solid line being the best fit with Eq. (4) for the E_0' CP and Eq. (5) for the E_2 CP. The parameters are also listed in Table II.

In Fig. 8 we show the temperature dependence of the phase angles ϕ for the E_1 transition, fitted with an excitonic line shape and a 2D CP, and for the E_0' and E_2 CP fitted with a 2D CP, respectively. The phase angles for the $E_1+\Delta_1$ CP are the same as for E_1. The parameter ϕ represents the mixture of contiguous CP's for the different transitions or the interaction with a background in the case of the excitonic line shape. Finally, the amplitudes A of the main structures observed are plotted versus temperature in Fig. 9.

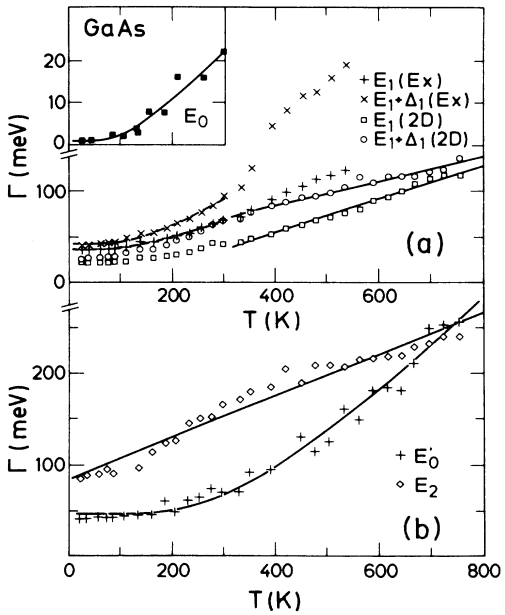

FIG. 7. Temperature dependence of the broadening parameters of the critical points. (a) Broadenings of the E_1 and $E_1+\Delta_1$ transitions, fitted with an excitonic (Ex) line shape up to 550 K and a 2D line shape. The solid lines are fits to the data which represent best the experimental line shape [for 20–300 K: fit to Eq. (4), for 300–760 K: linear fit]. The inset shows the broadening of the E_0 transition. (b) Broadening of the E_0' and E_2 CP's, together with the fit to Eq. (4) and a linear fit, respectively.

IV. DISCUSSION

Comparing our data for the dielectric function of GaAs at room temperature with those from Ref. 1 (see Fig. 2)

TABLE II. Values of the parameters obtained by fitting the Lorentzian broadening Γ of the critical points of GaAs versus temperature to the equation $\Gamma(T)=\Gamma_0[1+2/(e^{\Theta/T}-1)]+\Gamma_1$ or $\Gamma(T)=\Gamma_L+\gamma T$. Ex: CP fitted with excitonic, 2D: fitted with 2D line shape. The numbers in parentheses indicate error margins.

	Γ_1 (meV)	Γ_0 (meV)	Θ (K)	Γ_L (meV)	γ (10^{-4} eV K^{-1})	Temperature range (K)
E_0 (Ex)	−22(27)	23(29)	337(259)			20–300
E_1 (Ex)	0(fixed)	41(3)	293(26)			20–300
E_1 (2D)				−19(6)	1.84(11)	300–760
$E_1+\Delta_1$ (Ex)	0(fixed)	36(1)	356(17)			20–300
$E_1+\Delta_1$ (2D)				31(8)	1.34(15)	300–760
E_0' (2D)	−255(119)	300(123)	1013(218)			20–760
E_2 (2D)				84(8)	2.28(19)	20–760

the main differences occur in the uv spectral region and in the values of ϵ_2 at energies smaller than 2.5 eV. The last discrepancy should be due to the inherent poor accuracy of rotating analyzer ellipsometers for small values of ϵ_2. In this case, ϵ_2 is proportional to $\sin\Delta$ and Δ is close to $-\pi$.[1] However, rotating analyzer ellipsometers measure $\cos\Delta$ rather than $\sin\Delta$, so that the uncertainty in the determination of Δ is largest for $|\cos\Delta|\approx 1$. The differences in the higher photon-energy region could arise from the windows used for the cryostat. Although we have used high-quality stress-free fused quartz windows, a small systematic error is present in our measurements because of residual changes in the polarization of the light due to the windows. The changes have been estimated to be at worst $\delta(\psi)<0.3°$ and $\delta(\Delta)<0.7°$ in the uv spectral region.[56] This corresponds to a maximal uncertainty in the values of the dielectric function of $\delta(\epsilon_1)\approx 0.7$ and $\delta(\epsilon_2)\approx 0.9$ at 5 eV. These changes do not alter significantly the critical-point parameters, which are the subject of the present investigation.

A. E_0 and $E_0+\Delta_0$ transitions

The transitions of the lowest direct gap E_0 take place at the Γ point of the BZ between the Γ_8 valence-band and Γ_6 conduction-band states (double group notation).[87] The $E_0+\Delta_0$ transitions are between the Γ_7 splitoff valence-band state to the Γ_6 state. These transitions, however, are very weak, so that structure in the real part of the dielectric function is only visible to the naked eye at low temperatures for the E_0 transitions (see Fig. 3). In the second-derivative spectra $d^2\epsilon_1/d\omega^2$ it was possible to follow this structure up to 520 K, whereas the $E_0+\Delta_0$ structure could be analyzed only up to 200 K. In the ϵ_2 spectra because of the poor accuracy of our equipment at low ϵ_2 no significant change of ϵ_2 was observed in the E_0 and $E_0+\Delta_0$ region.

The E_0 transitions are dominated by an edge exciton whose binding energy is 4.2 meV.[6] Hence a fit of the second-derivative spectrum was performed using a Lorentzian line shape.

In Table III we have listed the energies of the interband critical points of GaAs for energies up to 5.5 eV, as obtained by various techniques and at several temperatures, together with our values from ellipsometry at 22, 85, 297, and 696 K. Our results agree well with those reported by other authors.

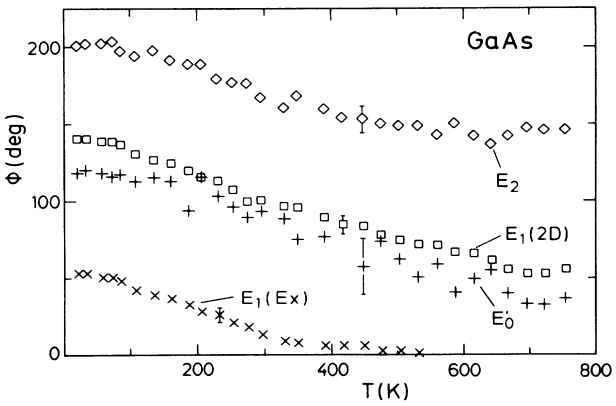

FIG. 8. Temperature dependence of the phase angle ϕ defined in Eq. (1) for the E_1 transitions, fitted with an excitonic, ×, and a 2D line shape, □. Also, phase angle ϕ for the E_0', +, and E_2, ◇ transitions.

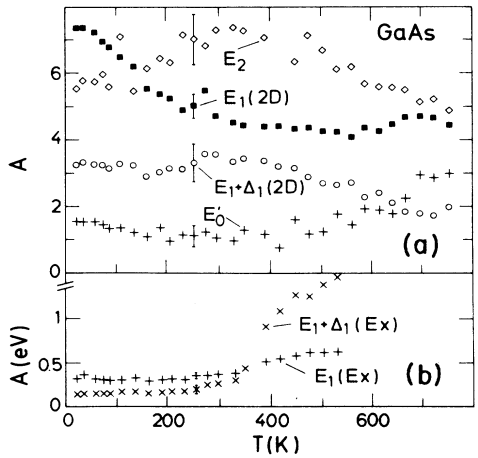

FIG. 9. Temperature dependence of the strength A, defined in Eq. (1). (a) Amplitudes of the E_1, ■; $E_1+\Delta_1$, ○; E_0', +; and E_2, ◇, transitions, all fitted with a 2D line shape. (b) Amplitudes of the E_1 and $E_1+\Delta_1$ transitions, fitted with an excitonic line shape.

TABLE III. Critical-point energies in GaAs at several temperatures. All energies are in eV. The numbers in parentheses indicate error margins.

Temperature (K)	E_0	$E_0+\Delta_0$	E_1	$E_1+\Delta_1$	E_0' region		E_2 region		
				Experiment					
1.6	1.5189[a]								
1.8	1.5188[b]								
2	1.5192[c]	1.859[t]							
4.2	1.5177[d]	1.859[d]	3.0439[d]	3.2636[d]	4.488[d]	4.529[d]	4.659[d]	4.937[d]	5.014[d]	5.137[d]
						4.712[d]	5.014[d]		5.339[d]	5.415[d]
5			3.017[aa]	3.245[aa]	4.44[aa]	4.60[aa]		5.11[aa]	5.91[aa]	
10	1.515[e]	1.856[u]								
21	1.515[e]									
22	1.5151(6)[f]	1.850(2)[f]	3.038(1)[f]	3.262(2)[f]	4.498(3)[f]	4.599(8)[f]	4.777(18)[f]	4.898(16)[f]		5.118(3)[f]
25	1.516[g]		3.101[g]	3.244[g]						
55	1.518[e]									
77	1.5114[h]		2.971[bb]	3.178[bb]	4.50[bb]	4.67[bb]		4.89[bb]		
80	1.46[i]	1.80[i]	2.95[i]	3.19[i]	4.5[i]	4.8[i]		5.05[i]	5.35[i]	
	1.511[j]		3.03[cc]	3.24[cc]	4.4[cc]					
	1.511[k]									
	1.5063(2)[f]	1.841(3)[f]	3.025(1)[f]	3.249(2)[f]	4.499(4)[f]			5.097(6)[f]		
90	1.511[e]									
100		1.845[u]								
110								5.03[ii]	5.9[ii]	
160	1.483[j]									
185	1.479[e]									
273	1.427[l]	1.763[l]	2.884[l]	3.111[l]	4.415[l]			4.95[l]		
296	1.426	1.784[k]	2.97[dd]	3.17[dd]				5.03[jj]	5.16[jj]	5.45[jj]
	1.43[m]	1.77[m]	2.89[m]	3.12[m]	4.44[m]		4.63[m]	4.99[m]	5.33[m]	
			2.96[m]	3.19[m]						
	1.4257[h]		2.91[ee]	3.12[ee]						
	1.427[n]	1.761[n]	2.898[n]	3.125[n]	4.46[n]		4.64[n]	4.99[n]	5.35[n]	
			2.963[n]	3.212[n]						
	1.420[o]	1.760[o]	2.90[ff]	3.13[ff]	4.45[ff]			5.04[ff]		
	1.435[e]		2.97[gg]	3.2[gg]						
	1.424[p]	1.745[u]	2.94[gg]	3.13[gg]						
	1.428[j]		2.9[hh]	3.1[hh]				5.0[hh]		
	$\Delta_0=0.340$[v]		2.904[v]	3.132[v]						
	$\Delta_0=0.35$[w]			$\Delta_1=0.24$[w]						

TABLE III. (*Continued*).

Temperature (K)	E_0	$E_0+\Delta_0$	E_1	$E_1+\Delta_1$	E_0' region		E_2 region	
			2.921[d]	3.135[d]				
			2.89[g]	3.12[g]				
	1.429(6)[f]		2.915(2)[f]	3.139(3)[f]	4.452(8)[f]		4.960(11)[f]	
473	1.350[q]							
500	1.33[r]	1.68[r]	2.91[r]	3.14[r]				
673	1.253[q]							
696			2.650(5)[f]	2.874(5)[f]	4.297(39)[f]		4.717(19)[f]	
873	1.147[q]							
973	1.090[q]							
					Theory			
	1.51[s]	1.86[s]	3.03[s]	3.25[s]	4.54[s]	4.7[s]	5.07[s]	5.28[s]
		$\Delta_0=0.35$[x]		$\Delta_1=0.22$[x]				
		$\Delta_0=0.34$[y]		$\Delta_1=0.21$[y]				
		$\Delta_0=0.32$[z]		$\Delta_1=0.20$[z]				
					4.42[kk]	4.60[kk]	4.36[kk]	5.0[kk]

[a]Reference 8.
[b]Reference 9.
[c]Reference 18.
[d]Reference 7.
[e]Reference 5.
[f]Present work.
[g]Reference 29.
[h]Reference 14.
[i]Reference 27.
[j]Reference 24.
[k]Reference 16.
[l]Reference 32.
[m]Reference 34, two structures for the E_1 and $E_1+\Delta_1$ CP.
[n]Reference 30, two structures for the E_1 and $E_1+\Delta_1$ CP.
[o]Reference 31.
[p]Reference 17.
[q]Reference 10.
[r]Reference 26.
[s]Reference 4.
[t]Reference 41.
[u]Reference 15.
[v]Reference 36.
[w]Reference 37.
[x]Reference 46.
[y]Reference 47.
[z]Reference 44.
[aa]Reference 39.
[bb]Reference 38.
[cc]Reference 25.
[dd]Reference 13.
[ee]Reference 33.
[ff]Reference 20.
[gg]Reference 11.
[hh]Reference 21.
[ii]Reference 28.
[jj]Reference 19.
[kk]Reference 43.

In order to compare the results for the temperature dependence of the E_0 gap we show in Table IV the linear temperature coefficients obtained both experimentally and theoretically by several authors, in most cases averaged between 100 and 300 K. The temperature shift for the $E_0+\Delta_0$ gap should be the same as for E_0 because of the intra-atomic nature of the spin-orbit splitting, a fact which is supported by earlier electroreflectance measurements between 25 and 300 K.[29]

The temperature dependence of the E_0 and $E_0+\Delta_0$ transitions was fitted with the Varshni equation [Eq. (3a)] as well as with Eq. (3b). In the case of the $E_0+\Delta_0$ CP the parameters β and Θ were forced to be the same as for the E_0 CP. In these fits, the effect of thermal expansion and electron-phonon interaction are not explicitly separated. This leads to an increase of the parameters β and Θ when compared with those for the pure electron-phonon interaction. Manoogian and Woolley[71] have suggested an equation to separate the effect of lattice dilation and electron-phonon interaction, based on a power law for the first and the Bose-Einstein statistical factor for the latter, identical to Eq. (3b). Moreover, they showed that the Varshni equation [Eq. (3a)] is a second-order approximation of Eq. (3b) and the parameter β is related to the Debye temperature Θ_D by $\beta=(\frac{3}{8})\Theta_D$. If we subtract from our data for the temperature dependence of the E_0 gap of GaAs the contribution of thermal expansion, as calculated in Ref. 69 from the experimental pressure coefficients, and refit the remaining contribution with the Varshni equation [Eq. (3a)], we obtain $\beta=127$ K, in good agreement with $(\frac{3}{8})\Theta_D=129$ K, when $\Theta_D=344$ K is used.[88]

TABLE IV. Linear temperature coefficients of critical-point energies in GaAs; all values in 10^{-4} eV/K. The numbers in parentheses indicate error margins.

$-dE_0/dT$	$-dE_1/dT$	$-dE_0'/dT$	$-dE_2/dT$
Experimental			
Between 100 and 300 K			
3.9[a]	5.3[g]	3.0[h]	3.6[g]
3.95[b]	4.8[h]	2.7(5)[e]	3.3[h]
3.9[c]	5.4[i]		6.3(4)[e]
3.7[d]	4.2[j]		
3.9(9)[e]	5.2(1)[e]		
Between 400 and 500 K			
4.9[d]	6.5(2)[e]	3.5(6)[e]	6.5(4)[e]
5.0(1.2)			
Theoretical			
Between 100 and 300 K			
4.45[a]	4.7[k]		3.7[k]
4.5[f]			3.5[l]
Between 400 and 500 K			
5.2[f]			

[a]Reference 23.
[b]Reference 14.
[c]Reference 70.
[d]Reference 10.
[e]Present work.
[f]Reference 69.
[g]Reference 39.
[h]Reference 20.
[i]Reference 20, for the $E_1+\Delta_1$ CP.
[j]Reference 13.
[k]Reference 49.
[l]Reference 48, within the Penn model.

We note that recently a calculation of the temperature dependence of the E_0 gap of GaAs has been performed[69] based on realistic band structure and lattice dynamics and including thermal expansion, Debye-Waller, and Fan terms. This calculation reproduced the experimental data: the temperature dependence becomes nonlinear at lower temperatures resulting in a decrease in the temperature coefficient which tends to zero for $T\rightarrow 0$. Also, the quantitative agreement is very good; a temperature coefficient between 100 and 300 K of -4.5×10^{-4} eV/K was obtained[69] in comparison with -3.9×10^{-4} eV/K from our ellipsometric results.

The broadening of the E_0 structure at 22 K, the lowest temperature reached with our cryostat, was determined to be 1 meV [see the inset of Fig. 7(a) and Table II]. This broadening is largely due to the limited experimental resolution of ~0.6 meV. It is known that there is a strong temperature dependence of the broadening all the way down to ~0 K. From reflectance measurements[41] a broadening <0.1 meV was found at 2 K, whereas the broadening parameter increases to about 0.8 meV at 30 K. Therefore we believe that our data at least at temperatures between 50 and 300 K are reasonable (except for the instrumental broadening of ~0.6 meV). At higher temperatures the E_0 structure becomes too weak to determine meaningful broadenings. This also applies to the $E_0+\Delta_0$ structure in the whole temperature range.

The negative value of Γ_1 for the E_0 transition, given in Table II can have no physical meaning. Indeed, Eq. (4) is based on the assumption of broadening by interband scattering via phonon emission and absorption whereas for the lowest gap only intraband scattering through phonon absorption is expected. In fact, it is possible to rewrite Eq. (4) with the fitting parameters for the E_0 transition as (in meV):

$$\Gamma(T)=-22+23(2n_\Theta+1) \quad (6a)$$

$$=1+46n_\Theta\ , \quad (6b)$$

where $n_\Theta=(e^{\Theta/T}-1)^{-1}$ is the phonon occupation number. The second term in Eq. (6b) corresponds to the increasing broadening with temperature solely through phonon absorption. The negative summand -22 is simply needed to remove the phonon emission part from Eq. (4).

B. E_1 and $E_1+\Delta_1$ transitions

The E_1 and $E_1+\Delta_1$ transitions take place along the Λ directions of the BZ,[4,7] where the valence and conduction bands are nearly parallel (compare Fig. 1). If they were strictly parallel, the E_1 and $E_1+\Delta_1$ transitions would be 2D CP's. Fits of the experimental line shape of these CP's have shown that for GaAs (Refs. 7 and 32) the 2D

model density of states yields the best representation. Recently, the CP's of Ge,[56] α-Sn,[58] and InSb (Ref. 57) have been investigated ellipsometrically as a function of temperature. Also for these materials the best fit was found with a 2D CP at all temperatures. Nevertheless, as already pointed out in Ref. 56, a conjunction of two 3D critical points nearly degenerate in energy (i.e., closer together than their broadening parameter Γ) cannot be distinguished from a 2D CP.

When fitting the second derivative spectrum $d^2\epsilon/d\omega^2$ of the E_1 and $E_1+\Delta_1$ structures at low temperatures with a 2D line shape, i.e., $n=0$ in Eq. (2), we noticed that the quality of the fit at the wings of the structure is rather poor whereas at higher temperatures (from $\sim$300 K) the fit is excellent everywhere. In Fig. 10 we illustrate this problem for a spectrum measured at 22 K. The dashed line shows the fit with the 2D line shape according to Eq. (2) ($n=0$). A phase angle of $\phi=141°$ was obtained which corresponds to a mixture of a 2D maximum and a saddle point.

The phase angle ϕ describes [Eq. (1)] a metamorphism of critical-point line shapes or Van Hove singularities due to excitonic effects by allowing a continuous admixture between two adjacent CP's (Ref. 84) with $\phi=0°,\ldots,360°$ in the case of a 3D and $\phi=0°,\ldots,270°$ for a 2D CP. When treated as uncorrelated one-electron transitions, the E_1 critical point should correspond to interband minima, i.e., to $\phi=0$. The excitonic metamorphism should transform ϕ into $0<\phi<90°$. Hence the value $\phi=141°$ obtained from our fit seems to be unphysical. Also, as shown in Fig. 10, the 2D representation of the E_1 transitions at low temperatures in GaAs is not wholly suitable to describe the experimental line shape. Similar conclusions can be made by examining modulated-reflectivity measurements.[27,38,89]

Many-particle effects on critical points in the interband continuum of semiconductors have been treated with similar models as for the bound excitons.[90] One of them is the effective-mass approximation (EMA). For the M_1-type CP, i.e., for the so-called saddle-point exciton, it was possible to include the untruncated Coulomb interaction screened by the macroscopic dielectric constant ϵ_0,[91,92] using the adiabatic approximation. This method is accurate if one of the principal reduced masses is much larger ($\approx\infty$) than the two others. The starting point is then a two-dimensional Wannier exciton.

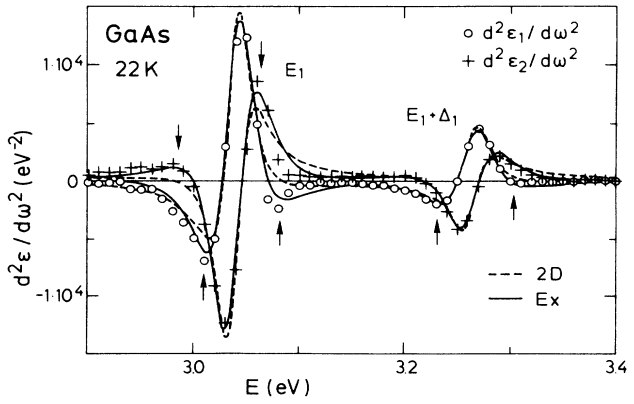

FIG. 10. Second derivatives of ϵ_1 and ϵ_2 with respect to energy in the E_1 spectral region for GaAs at 22 K. The dashed lines represent fits with a 2D CP, the solid lines to an excitonic line shape. The arrows indicate regions where an improvement of the fit is achieved by using an excitonic instead of a 2D line shape.

An approach based on a Frenkel or tight-binding approximation is the Koster-Slater model.[2,91,93] Within this model, the Coulomb interaction is truncated beyond a certain value of the electron-hole separation. The simplest assumption is that of a Koster-Slater contact interaction potential $V(\mathbf{r})=-\delta(\mathbf{r})g$ which is equal to zero except when the Wannier electron and hole are in the same unit cell. Velicky and Sak[91] have shown that the absorption at an M_1 CP is enhanced and weakened at an M_2 CP by introducing an attractive electron-hole interaction. The contact-interaction can be parametrized to describe experimental deviations of the measured dielectric function from the one-electron picture[2,91,94]

$$\epsilon(\omega)-1=\frac{\tilde{\epsilon}(\omega)-1}{1-g[\tilde{\epsilon}(\omega)-1]},\quad g>0\,, \tag{7}$$

where $\tilde{\epsilon}(\omega)$ is the one-electron dielectric function and the parameter g is proportional to the depth of the assumed square-well potential.

In a similar manner, also replacing the Coulomb potential by a finite-range potential, it was shown[84] that the effect of such a potential on a singular line shape in the vicinity of an M_i-type CP is to mix the M_i line shape with the M_{i+1}-type CP (with $M_4\equiv M_0$). These results, applied to the one-electron line shape of CP's provide the theoretical underpinning of Eq. (7) which can be transformed into Eq. (1) provided g is small.

Recently, the optical response of a semiconductor has been calculated using a local-orbital treatment of the two-particle Green's function for the electron-hole interaction.[95,96] In these calculations the experimental ϵ_2 spectra around E_1 and $E_1+\Delta_1$ were shown to be enhanced above those within the one-electron approximation. It was also shown that a qualitative agreement between the experimental and calculated ϵ_2 spectra was only achieved when screened electron-hole interaction as well as local-field corrections are included in the calculations.

Another, quite general approach to the treatment of excitons at the fundamental edge, as well as in the continuum, was developed by Stahl.[97–99] Here, the exciton polariton, which behaves as a quasiboson field within a linear-response theory, is described by a coherent macroscopic pair wave function, whose linear response to an electric field is given by a wave equation in electron-hole configuration space. This approach can in principle handle saddle-point exciton polaritons with an unrestricted range of mass ratios, in contrast to the EMA of Refs. 91 and 92. It allows simultaneously the calculation of the real and imaginary part of the susceptibility as well as a combined treatment of the exciton resonances and the continuum.[97] This approach has been applied to the M_1-type E_1 CP of ZnTe, the calculated line shapes agree well with the experimental ones.[100] Unfortunately, it seems that no analytical line shape suitable to fit CP line shapes is obtained

within this method.[97]

The only two analytical equations which include excitonic effects, Eq. (1) with a phase factor $e^{i\phi}$ and Eq. (7) with the g factor in the denominator, are based on short-range electron-hole interaction. Thus we have also tried to use Eq. (7) for the fit of our second-derivative spectra of $\epsilon(\omega)$ with respect to the photon energy with the equations:

$$\frac{d^2\epsilon}{d\omega^2}=\frac{\frac{d^2\tilde{\epsilon}(A,E,\Gamma)}{d\omega^2}}{[1-g(\epsilon^*-1)]^2}+\frac{2g\left[\frac{d\tilde{\epsilon}(A,E,\Gamma)}{d\omega}\right]^2}{[1-g(\epsilon^*-1)]^3} . \quad (8)$$

The one-electron dielectric function not differentiated with respect to the photon energy in the denominator of Eq. (8) is labeled as ϵ^*. However, a difficulty arises in obtaining the *one-electron* dielectric function ϵ^* to be inserted into Eq. (7): This function is not directly measurable. We have tried the following quasi-self-consistent fit procedure.

(1) Determine g by using the experimental values of $\epsilon(\omega)$ (see Figs. 3 and 4) for ϵ^* in the denominator of Eq. (8) and for the derivatives in the numerator the 2D one-electron line shape of Eq. (2) with the three parameters A (amplitude), E (CP energy), and Γ (broadening) as fit parameters and $\phi=0$ (phase angle) as fixed parameter. $\phi=0$ was chosen because for the fit with Eq. (2) ($n=0$), ϕ decreased monotonically from $\phi=141°$ at 22 K to $\phi=56°$ at 754 K (see Fig. 8); excitonic effect should disappear for $\phi=0$.

(2) With the g factor obtained from step (1) determine a new quasi-one-electron dielectric function $\tilde{\epsilon}^*(\omega)$ using the inversion of Eq. (7):

$$\tilde{\epsilon}^*-1=\frac{\epsilon^*(\omega)-1}{1+g[\epsilon^*(\omega)-1]} , \quad (9)$$

where $\epsilon^*(\omega)$ is the dielectric function used in the denominator of Eq. (8) when performing step (1).

(3) With the new quasi-one-electron dielectric function $\tilde{\epsilon}^*$ in the denominator of Eq. (8) again determine the parameters A, E, Γ, and g of the two CP's.

(4) With the new g factor determine again a corrected quasi-one-electron dielectric function and repeat step (3).

Unfortunately, the values of g obtained with this procedure did not converge. After the first fit the value of g was 0.039 (2). It increased after every step by about $\Delta g=0.020$ so that for example after the fifth step we obtained $g=0.120$ (1). At the same time the quality of the fit to the data in Fig. 10 improved only slightly. The residual sum of squares which measures the deviation of the fit to the experimental values, decreased only from 1×10^6 after the first step to 0.4×10^6 after the fifth step in the energy range chosen for the fit (2.8–3.5 eV). This was no improvement with respect to the simple fit with a 2D line shape from Eq. (2), where the residual sum of squares was 0.4×10^6. In addition the magnitude of the quasi-one-electron dielectric function $\tilde{\epsilon}^*(\omega)$ obtained in step (2) decreases with every step of the procedure and its structure is flattened. For example, after five steps the real part of $\tilde{\epsilon}^*(\omega)$ lies between 6 and 8 and the imaginary part between 1 and 3 in the 2.8–3.5-eV photon-energy range. These values are much too low for the one-electron dielectric function and decrease even further when more fit steps are performed. In theoretical calculations of the dielectric function in the approximation of noninteracting electron-hole pairs in the case of Si (Ref. 95) and GaP (Ref. 96) the values of the imaginary part of the dielectric function at E_1 are found to be at most only about a factor of 2 lower than the experimental $\epsilon_2(E_1)$.

Note that the one-electron dielectric function ϵ^* in the denominator of Eq. (8) cannot be obtained from the parameters A, E, and Γ, which are determined from the fit to the derivative spectra, because the constant background has been removed. In summary we conclude that the contact interaction as described by Eq. (7) is not appropriate for large phase shifts which are beyond 90°, as it would be necessary to fit our CP line shapes for the E_1 and $E_1+\Delta_1$ transitions over the whole measured temperature range. Finally we would like to mention that also for a 3D line shape, assuming that the one-electron dielectric function corresponds to a M_1 CP, yielded a fit of only poor quality with $g=0.040$ (8) and a residual sum of squares of 2×10^6. The intriguing question thus remains as to why Eq. (1) gives such good representation of the experimental data. Its only known link with theory is through Eq. (7) for small values of g.[2,91,94] For large values of g this link breaks down, Eq. (7) has been shown to represent the data poorly and nevertheless Eq. (1) represents them well.

Although it is desirable to fit the CP's with the same model over the whole temperature range, we have found that at temperatures up to 300 K the best fit was performed with a Lorentzian line shape, i.e., with $n=-1$ in Eq. (1). At room temperature the quality of the fit with a Lorentzian and a 2D line shape is about the same. At higher temperatures the 2D line shape yields the better result.

In the case of a Lorentzian line shape [Eq. (1) or (2), $n=-1$] the phase factor $e^{i\phi}$ can be interpreted as a coupling parameter between the discrete exciton interacting with an overlapping continuum of interband transitions. In this case the resulting line shape is more commonly described by the so-called Fano-Breit-Wigner profile[73] which can be written in the following form:

$$\mathrm{Im}F(\omega)=B\frac{|Q+\zeta|^2}{\zeta^2+1} , \quad (10)$$

where ζ is a reduced frequency $\zeta=(\omega-E)/\Gamma$, Γ the linewidth parameter, Q a complex parameter, and B the amplitude.

The complete function $F(\omega)$ is given by

$$F(\omega)=\sigma-B\frac{|Q+\zeta|^2}{\zeta+i}=\sigma-B(\zeta-i)\frac{|Q+\zeta|^2}{\zeta^2+1} . \quad (11)$$

Here we have assumed Q to be real which can always be done by adding an additional noninteracting scattering continuum σ.[73] By comparison of the Fano-Breit-Wigner profile [Eq. (11)] and the Lorentzian line shape [Eq. (1) for $n=-1$] in the second derivative, one can find the following relationships between the parameters:

$$Q = -\cot\phi - \frac{1}{\sin\phi} ,$$
$$\frac{A}{B} = (Q^2-1)^2 + 4Q^2 , \tag{12}$$

i.e., the line-shape parameter Q and the amplitude B from the Fano-Breit-Wigner profile [Eq. (11)] can be determined from A and ϕ of Eq. (1).

Obviously, the E_1 and $E_1+\Delta_1$ transitions in GaAs are an example for the coexistence of local and band characters in the optical spectra of solids, as discussed by Toyozawa *et al.*[84] For temperatures smaller than 300 K, their line shape is described by a quasilocal state superposed upon the background of continuous states which leads to Fano-Breit-Wigner interference effects. On the other hand, for temperatures above 300 K, the line shape of the E_1 and $E_1+\Delta_1$ CP's is better described by the modification of the Van Hove singularity due to local perturbations, as done in the general line-shape formula [Eq. (1)] by the phase angle ϕ.

The change from local to band character is supported when looking at the phase angles and amplitudes obtained from the line-shape fits. In Fig. 8 the phase angle for the fit with a Lorentzian decreased from 55° at 22 K to near zero above 300 K. A phase angle of zero corresponds to no interaction of the discrete state with the continuum. At higher temperatures ($T>300$ K) the picture of a continuum influenced by a discrete excitation, expressed by a metamorphism of the 2D CP line shape, becomes more suitable. At 300 K a phase angle of $\phi=100°$ is obtained which decreases to about 50° at 750 K, i.e., the line shape is a mixture between a 2D saddle point and a minimum.

The amplitudes of the E_1 and $E_1+\Delta_1$ CP (see Fig. 9) are nearly constant in the 20—250 K temperature range when fitted with a Lorentzian and then increase, a fact which indicates a change in the character of the transitions. For the fit of the E_1 CP with a 2D line shape we observed a decrease of the amplitudes with temperature remaining about constant for $T>300$ K (see Fig. 9).

From measurements on Ge (Ref. 56) and InSb,[57] however, it is known that the ratio of the amplitudes $A_{E_1}/A_{E_1+\Delta_1}$ for a 2D CP shows only a weak dependence on temperature, so that the decrease of A_{E_1} at $T<300$ K must reflect the inappropriate description by the 2D line shape. We finally note that evidence of the excitonic nature of the E_1 and $E_1+\Delta_1$ transitions of CdTe has been shown by analyzing thermoreflectance spectra.[89]

Over the whole temperature range the E_1 and $E_1+\Delta_1$ CP's have been fitted simultaneously, assuming for both the same phase angle ϕ and a temperature-independent spin-orbit splitting $\Delta_1=224$ meV, as determined from the low-temperature spectra. This is justified by the intraatomic nature of the so splitting as much as by earlier measurements,[29] also on other materials.[56–58] In Table III we give a comparison of the E_1 and $E_1+\Delta_1$ CP energies at several temperatures. Differences between the data might be due to the fact that for the evaluation of unsymmetric peaks, e.g., in the reflectivity spectrum, a line-shape analysis is necessary because the maximum position does not correspond to the real CP energy.

Figure 6 shows the temperature dependence of the E_1 CP energies. Those for the $E_1+\Delta_1$ transitions are shifted by 224 meV to higher energies. The solid line represents the best fit to the Varshni formula [Eq. (3a)], the dashed line to Eq. (3b). As already pointed out in the preceding section, the parameter β in Eq. (3a) and Θ in Eq. (3b), respectively, are not directly related to an average frequency of the phonons involved in the electron-phonon interaction which causes the shift of the CP's with temperature.

In Fig. 7 we show the temperature dependence of the broadening parameter Γ of the E_1 and $E_1+\Delta_1$ transitions obtained from the fit with a Lorentzian excitonic (Ex) line shape as well as with a 2D line shape. The broadening depends on the assumed line shape. To describe the temperature dependence for $T<300$ K (Lorentzian line shape) Eq. (4) was used, whereas for $T>300$ K a linear fit [Eq. (5)] was performed, represented by the solid lines in Fig. 7.

The temperature dependence of the broadening of the CP's is due to electron-phonon interaction and can be described by the imaginary part of the self-energy, whose real part represents the energy shift of the bands.[68] A constant broadening Γ_1 in Eq. (4) is due to additional temperature-independent mechanisms (Auger processes, electron-electron interaction, impurities, surface scattering, and also instrumental effects). This parameter, however, turned out to be zero within the error of the fit. It was thus set equal to zero. In contrast to the case of the *energy shift*, the parameter Θ in Eq. (4) corresponds to an average phonon frequency obtained after weighting the phonon density of states by an electron-phonon spectral function.[68] The value of $\Theta=293$ K for E_1 and $\Theta=356$ K for $E_1+\Delta_1$ indicates that mainly optical phonons are responsible for the broadening, the energy of the LO phonon at Γ corresponding to a temperature of about 420 K.

The temperature Θ obtained when fitting the temperature dependence of the Γ of a CP is not necessarily the same as the one for the shift of the corresponding CP energies, after correcting for the thermal expansion contribution. Calculations of the electron-phonon spectral functions for Si and Ge have shown that for the energy shift due to electron-phonon interaction acoustical as well as optical phonons contribute (see e.g., Figs. 1 and 2 of Ref. 67), whereas for the broadening of the CP mainly optical phonons are responsible (see Figs. 2 and 3 of Ref. 68). This must lead to a higher average phonon frequency Θ from the fit of Eq. (4) to the broadening parameters than for the electron-phonon contribution of the energy shifts with temperature. This conjecture is borne out by comparing Tables I and II.

The amplitudes of the E_1 and $E_1+\Delta_1$ excitons are nearly constant in the 20—250 K temperature range (see Fig. 9). They are for E_1 about a factor of 2 larger than for $E_1+\Delta_1$. They can be estimated theoretically by writing the dielectric function for the interband contribution due to the exciton:[2]

$$\epsilon(\omega) = 1 + 4\pi \sum_j \frac{F^j}{\omega_j - (\omega + i\eta)^2} , \tag{13}$$

where ω_j represents the energy of any excited electron-hole pair with respect to the ground state $|0\rangle$ and F^j is

the oscillator strength for transitions from the ground state to an excited pair state

$$F^j=\frac{2\left|\left\langle j\left|\sum_i p^i\right|0\right\rangle 2\right|^2}{\omega_j} . \tag{14}$$

Using the relationship[2]

$$\left\langle j\left|\sum_i p^i\right|0\right\rangle=\phi(0)\langle c\,|\,p\,|\,v\rangle \tag{15}$$

and taking into account the geometry for the transitions along the eight $\langle 111\rangle$ directions, assuming that the transitions take place over a distance $\Delta k=\pi\sqrt{3}/a_0$ (a_0 is the lattice constant) and $|\phi(0)|^2$ for the 2D case given by[2]

$$|\phi(0)|^2=\frac{16m_d^3}{\pi\epsilon^3} , \tag{16}$$

we obtain

$$\epsilon(\omega)=\frac{16\pi}{\omega^2}\frac{8}{3}P^2\frac{\pi\sqrt{3}}{a_0}\frac{1}{2\pi}\frac{16m_d^3}{\pi\epsilon_s^3}\frac{1}{\omega-\omega_0+i\Gamma} , \tag{17}$$

where $P=\langle c\,|\,p\,|\,v\rangle$, m_d is the reduced effective mass, and ϵ_s is the dielectric constant responsible for the screening of the Coulomb potential of the exciton interaction. The matrix element P in zinc-blende materials can be assumed to be:[101] $P\approx 2\pi/a_0$. The reduced effective masses can be calculated with the $\mathbf{k}\cdot\mathbf{p}$ method:[101]

$$\frac{1}{m_d(E_1)}\approx\frac{3P^2}{\omega_1+\Delta_1/3}, \quad \frac{1}{m_d(E_1+\Delta_1)}=\frac{3P^2}{\omega_1+2\Delta_1/3} . \tag{18}$$

The amplitude of the E_1 and $E_1+\Delta_1$ excitonic transitions now follow:

$$A_{E_1}=\frac{64\sqrt{3}}{81\pi^4}\frac{a_0^3}{\omega^2\epsilon_s^3}(\omega_1+\Delta_1/3)^3 ,$$
$$A_{E_1+\Delta_1}=\frac{64\sqrt{3}}{81\pi^4}\frac{a_0^3}{\omega^2\epsilon_s^3}(\omega_1+2\Delta_1/3)^2 . \tag{19}$$

With the parameters $a_0=5.653$ Å. $\omega_1=\omega=3.038$ eV, $\Delta_1=0.224$ eV, and $\epsilon_s=12.5$ for the static dielectric constant we obtain the values $A_{E_1}=0.029$ eV and $A_{E_1+\Delta_1}=0.027$ eV, one order of magnitude less than the experimental values ($A_{E_1}=0.32$ eV, $A_{E_1+\Delta_1}=0.15$ eV).

In Eq. (19) the amplitude, however, is strongly dependent on the value of ϵ_s, i.e., on the screening of the Coulomb potential. A quantitative calculation of the space-dependent microscopic dielectric function $\tilde{\epsilon}(r)$ (Ref. 102) shows that for GaAs at a distance of about five Bohr radii from the nucleus the value of $\tilde{\epsilon}(r)$ begins to decrease from the long-wavelength infrared value of 10.9 down to one for the unscreened potential. If we assume that the "Bohr radius" of the exciton wave function is smaller than the lattice constant, a smaller value of ϵ_s should be used for the theoretical estimate of the amplitude. The experimental value ($A_{E_1}=0.32$ eV) is obtained with Eqs. (19) for $\epsilon_s=5.6$. In the calculation of Ref. 102 this corresponds to a radius of 1.2 Å, half the bond length in GaAs (2.45 Å).

The amplitudes for 2D E_1 and $E_1+\Delta_1$ transitions, assumed in the 300—750 K interval, can be calculated in the one-electron approximation with[101,103]

$$A_{E_1}\approx\frac{44(E_1+\Delta_1/3)}{a_0E_1^2}=2.8 ,$$
$$A_{E_1+\Delta_1}\approx\frac{44(E_1+2\Delta_1/3)}{a_0(E_1+\Delta_1)^2}=2.5 , \tag{20}$$

where the lattice constant a_0 is in Å and the energies E_1 and Δ_1, in eV, were taken at 400 K. From our fits at 400 K we found $A_{E_1}\approx 4.4$ and $A_{E_1+\Delta_1}\approx 3.4$ which corresponds to a ratio of $A_{E_1}/A_{E_1+\Delta_1}=1.3$. An improvement of the already good theoretical estimate is possible by including a correction for terms linear in $\mathbf{k}$ for $\mathbf{k}$ perpendicular to $\langle 111\rangle$. Calculations for Si (Refs. 104 and 105) and GaAs (Ref. 106) have shown that these terms increase the strength of the E_1 transition relative to the $E_1+\Delta_1$. If we use an average matrix element Π of $\mathbf{p}$ equal to that for Si ($\Pi\sim 0.1$ bohr^{-1}, Ref. 104), we get $A_{E_1}=3.0$ and $A_{E_1+\Delta_1}=2.3$. The calculated ratio $A_{E_1}/A_{E_1+\Delta_1}=1.3$ is in good agreement with the experimental one (also 1.3) at 400 K. The differences in the absolute magnitudes of calculated and experimental A_{E_1}'s can be attributed to excitonic interactions.[95,96]

Linear temperature coefficients, calculated from the fit parameters for the Varshni equation [Eq. (3a)] are given in Table IV for the temperature ranges 100—300 K and 400—500 K, together with other data from the literature.

C. E_0' and E_2 transitions

In the energy range of 4.2—5.5 eV there is an accumulation of interband CP's for GaAs. In high-resolution electroreflectance measurements[7] at 4.2 K a triplet of CP's was identified and attributed to transitions at the Γ point: $E_0'(\Gamma_8^v\rightarrow\Gamma_7^c)$ at 4.488 eV, $E_0'+\Delta_0'(\Gamma_8^v\rightarrow\Gamma_8^c)$ at 4.659, and $E_0'+\Delta_0'+\Delta_0(\Gamma_7^v\rightarrow\Gamma_8^c)$ at 5.014 eV (for the notation see Fig. 1). Also, a doublet $E_0'(\Delta)$ and $E_0'+\Delta_0'(\Delta)$, attributed to transitions along the $\langle 100\rangle$ directions (Δ line) of the BZ with energies of 4.529 and 4.712 eV, was found.

The E_2 complex was attributed to four transitions at the X point ($X_7^v\rightarrow X_6^c$ with 4.937 eV, $X_6^v\rightarrow X_6^c$ with 5.014 eV, $X_7^v\rightarrow X_7^c$ with 5.339 eV, and $X_8^v\rightarrow X_7^c$ with 5.415 eV). A further E_2 transition with Σ symmetry (5.137 eV) should take place in an extended region of the BZ.[7]

From nonlocal pseudopotential calculations[4] one expects four CP's in the 4.2-5.5 eV energy region: $\Delta_5^v\rightarrow\Delta_5^c$ at (0.1,0,0) (in units of $2\pi/a_0$), 4.54-eV energy, and along the same symmetry line, 4.70-eV energy. From a plateau located near (0.75,0.25,0.25) in the BZ a CP at 5.07 eV should arise. At the X point a CP with an energy of 5.28 eV is expected. In our second-derivative spectrum of the dielectric function at 22 K, shown in Fig. 5, we have performed a fit assuming five structures in the 4.2-5.5 eV energy range. We have identified the strong structure at 4.498 eV with the E_0' transition, where $E_0'(\Gamma)$ and $E_0'(\Delta)$ are not resolved, and the other pronounced structure at

5.118 eV to an E_2 CP, labeled $E_2(\Sigma)$ in Fig. 5, whose contribution seems mainly to arise from points along Σ and the plateau near (0.75,0.25,0.25).[4,7] Another, much weaker E_2 CP at 4.898 eV, labeled $E_2(X)$ in Fig. 5, should be attributed to $X_7^v \rightarrow X_6^c$ transitions. Two further weak CP's at 4.599 and 4.777 eV are probably due to $E_0'+\Delta_0'$ transitions at the Γ point and along the Δ lines, but the assignment of these features is less certain due to the deviation of about 60 meV from the value obtained in Ref. 7. Possibly the differences arise from an artifact in the fit and the assumed dimensionality of the CP line shapes, all chosen to be 2D. In Table III we give a comparison of the CP energies available in the literature with our results at several temperatures.

When going to higher temperatures only the two main structures E_0' and E_2 could be distinguished. Figure 6 shows the temperature dependence of the E_0' and E_2 energies, where both are fitted together with a 2D line shape which gave the best representation of the experimental data over the whole temperature range. The E_0' CP shifts less than the E_2 counterparts; the linear temperature coefficients are -2.7×10^{-4} eV/K for E_0' and -6.3×10^{-4} eV/K for E_2 in the 100–300 K temperature range. The larger shift of E_2 with respect to the E_0' CP seems to be a general fact, also observed for Ge (Ref. 56) and InSb.[57] The temperature dependence of E_2 is nearly linear, only a few points at low temperature cause a small quadratic contribution, as is evident from the small parameter $\beta=43$ K obtained through the fit with the Varshni relation [Eq. (3a)].

The fit of the temperature dependence of the broadening parameters of the E_0' to Eq. (4), shown in Fig. 6, yields a negative value for Γ_1 and an average phonon frequency of 1013 K which is nearly a factor of 2.5 higher than the highest phonon energy in GaAs ($\sim$420 K). We believe that this is an artifact due to the complicated structure of the E_0' transitions near the Γ point.

Individual bands, contributing to the broadening, can shift differently with temperature and thus the number of intermediate states for the interband scattering of the electrons changes. This can cause an anomalous behavior of the broadening. Similar arguments may be involved for the E_2 transitions. We have described their temperature dependence by a straight line because of the large scatter of the data.

The phase angles $\phi(E_0')$ and $\phi(E_2)$, displayed in Fig. 8, decrease with increasing temperature nearly by the same amount as in the case of the E_1 and $E_1+\Delta_1$ transitions. This suggests that also for the E_0' and E_2 CP excitonic effects are important. However, the complicated character of these CP's cautions us against attributing this fact purely to excitonic interaction.

In Table IV, we compare the linear temperature coefficients, obtained from our data, with those from other authors. We note that our value of -6.3×10^{-4} eV/K from a detailed line-shape analysis of the E_2 structure in the dielectric function is about 2 times higher than those found with the wavelength-modulation[39] and electroreflectance[20] techniques.

V. CONCLUSIONS

Data for the dielectric function of GaAs in the 1.3–5.5 eV range have been presented for several temperatures between 20 and 750 K. A detailed analysis of the critical points has been performed, leading to the temperature dependence of critical-point energies, amplitudes, Lorentzian widths, and phase angles. Perhaps the most interesting result obtained is the fact that the E_1 and $E_1+\Delta_1$ critical points are best fitted below room temperature by a Fano-modified Lorentzian line shape, thus confirming that these transitions are mainly a strongly localized excitonic resonance. An analysis of the strength of these excitonic transitions suggests a deviation from Wannier behavior in the form of central cell localization and thus a deep (rather than shallow) nature for these excitons. Such transitions may depend critically on the parameters of the semiconductor.[107] It has been observed recently to be less pronounced in InP,[108] another more ionic material of the family.

ACKNOWLEDGMENTS

One of us (M.G.) acknowledges financial support of Caixa de Pensions "la Caixa," Barcelona (Spain). We would like to thank W. Neu for help with the cryostat, G. Kisela and co-workers at the Max-Planck-Institut for sample preparation, and M. Bleder and A. Birkner for help with the construction of the ellipsometer. We would also like to thank H. Hirt, M. Siemers, and P. Wurster for expert technical help and S. Gopalan for a critical reading of the manuscript.

*Permanent address: First Laboratory of Physics, Aristotle University of Thessaloniki, Thessaloniki, Greece.

[1]D. E. Aspnes and A. A. Studna, Phys. Rev. B **27**, 985 (1983).
[2]M. Cardona, *Modulation Spectroscopy* (Academic, New York, 1969).
[3]D. E. Aspnes, in *Handbook on Semiconductors,* edited by M. Balkanski (North-Holland, Amsterdam, 1980), Vol. 2, Chap. 4A.
[4]J. R. Chelikowsky and M. L. Cohen, Phys. Rev. B **14**, 556 (1976).
[5]M. D. Sturge, Phys. Rev. **127**, 768 (1962).
[6]D. D. Sell, Phys. Rev. B **6**, 3750 (1972).
[7]D. E. Aspnes and and A. A. Studna, Phys. Rev. B **7**, 4605 (1973).
[8]D. Bimberg and W. Schairer, Phys. Rev. Lett. **28**, 442 (1972).
[9]A. M. White, P. J. Dean, L. L. Taylor, R. C. Clarke, D. J. Ashen, and J. B. Mullin, J. Phys. C **5**, 1727 (1972).
[10]M. B. Panish and H. C. Casey, Jr., J. Appl. Phys. **40**, 163 (1969).
[11]K. L. Shaklee, F. H. Pollak, and M. Cardona, Phys. Rev. Lett. **15**, 883 (1965).
[12]R. Braunstein and E. O. Kane, J. Phys. Chem. Solids **23**, 1423 (1962).
[13]M. Cardona and G. Harbeke, J. Appl. Phys. **34**, 813 (1963).

[14]M. Zvara, Phys. Status Solidi **36**, 785 (1969).
[15]W. Kauschke, M. Cardona, and E. Bauger Phys. Rev. B **35**, 8030 (1987); (unpublished).
[16]V. V. Sobolev, V. I. Donetskikh, and E. F. Zagainov, Fiz. Tekh. Poluprovodn. **12**, 1089 (1978) [Sov. Phys.—Semicond. **12**, 646 (1978)].
[17]D. D. Sell, H. C. Casey, Jr., and K. W. Wecht, J. Appl. Phys. **45**, 2650 (1974).
[18]D. D. Sell, S. E. Stokowski, R. Dingle, and J. V. Di Lorenzo, Phys. Rev. B **7**, 4568 (1973).
[19]S. S. Vishnubhatla and J. C. Woolley, Can. J. Phys. **46**, 1769 (1968).
[20]A. G. Thompson, J. C. Woolley, and M. Rubenstein, Can. J. Phys. **44**, 2927 (1966).
[21]H. Ehrenreich, H. R. Philipp, and J. C. Phillips, Phys. Rev. Lett. **8**, 59 (1962).
[22]M. Cardona and D. L. Greenaway, Phys. Rev. **125**, 1291 (1962).
[23]J. Camassel and D. Auvergne, Phys. Rev. B **12**, 3258 (1975).
[24]J. Camassel, D. Auvergne, and H. Mathieu, J. Appl. Phys. **46**, 2683 (1975).
[25]S. O. Sari and S. E. Schnatterly, Surf. Sci. **37**, 328 (1973).
[26]S. G. Dzhioeva, V. S. Ivanov, and V. B. Stopachinskii, Fiz. Tekh. Poluprovodn. **3**, 1316 (1969) [Sov. Phys.—Semicond. **3**, 1096 (1970)].
[27]E. Matatagui, A. G. Thompson, and M. Cardona, Phys. Rev. **176**, 950 (1968).
[28]G. Guizzetti, L. Nosenzo, E. Reguzzoni, and G. Samoggia, Phys. Rev. B **9**, 640 (1974).
[29]T. Nishino, M. Okuyama, and Y. Hamakawa, J. Phys. Chem. Solids **30**, 2671 (1969).
[30]A. G. Thompson, M. Cardona, K. L. Shaklee, and J. C. Woolley, Phys. Rev. **146**, 601 (1966).
[31]C. Alibert, S. Gaillard, M. Erman, and P. M. Frijlink, J. Phys. (Paris) Colloq. **44**, C10—229 (1983).
[32]S. F. Pond and P. Handler, Phys. Rev. B **8**, 2869 (1973).
[33]J. M. Wrobel, J. L. Aubel, U. K. Reddy, S. Sundaram, J. P. Salerno, and J. V. Gormley, J. Appl. Phys. **59**, 226 (1986).
[34]M. Cardona, K. L. Shaklee, and F. H. Pollak, Phys. Rev. **154**, 696 (1967).
[35]D. E. Aspnes, C. G. Olson, and D. W. Lynch, Phys. Rev. B **12**, 2527 (1975).
[36]E. W. Williams and V. Rehn, Phys. Rev. **172**, 798 (1968).
[37]K. L. Shaklee, M. Cardona, and F. H. Pollak, Phys. Rev. Lett. **16**, 48 (1966).
[38]M. Welkowsky and R. Braunstein, Phys. Rev. B **5**, 497 (1972).
[39]R. R. L. Zucca and Y. R. Shen, Phys. Rev. B **1**, 2668 (1970).
[40]J. P. Walter, R. R. L. Zucca, M. L. Cohen, and Y. R. Shen, Phys. Rev. Lett. **24**, 102 (1970).
[41]D. D. Sell, in *Proceedings of the 11th International Conference on the Physics of Semiconductors, Warsaw, 1972,* edited by M. Miasek (Elsevier, Amsterdam and PWN-Polish Scientific Publishers, Warsaw, 1972).
[42]M. L. Cohen and T. K. Bergstresser, Phys. Rev. B **141**, 789 (1966).
[43]F. H. Pollak, C. W. Higginbotham, and M. Cardona, J. Phys. Soc. Jpn. Suppl. **21**, 20 (1966).
[44]F. Herman, R. L. Kortum, C. D. Kuglin, and J. P. Van Dyke, Methods Comput. Phys. **8**, 193 (1968).
[45]G. B. Bachelet and N. E. Christensen, Phys. Rev. B **31**, 879 (1985), and references therein.
[46]D. J. Chadi, Phys. Rev. B **16**, 790 (1977).
[47]G. G. Wepfer, T. C. Collins, and R. N. Euwema, Phys. Rev. B **4**, 1296 (1971).
[48]P. Y. Yu and M. Cardona, Phys. Rev. B **2**, 3193 (1970).
[49]Y. F. Tsay, B. Gong, S. S. Mitra, and J. F. Vetelino, Phys. Rev. B **6**, 2330 (1972).
[50]D. Auvergne, J. Camassel, H. Mathieu, and M. Cardona, Phys. Rev. B **9**, 5168 (1974).
[51]P. B. Allen and V. Heine, J. Phys. C **9**, 2305 (1976).
[52]M. Schlüter, G. Martinez, and M. L. Cohen, Phys. Rev. B **12**, 650 (1975).
[53]P. B. Allen, Phys. Rev. B **18**, 5217 (1978); B. Chakraborty and P. B. Allen, *ibid.* **18**, 5225 (1978).
[54]H. Y. Fan, Phys. Rev. **82**, 900 (1951).
[55]M. L. Cohen, Phys. Rev. **128**, 131 (1962).
[56]L. Viña, S. Logothetidis, and M. Cardona, Phys. Rev. B **30**, 1979 (1984).
[57]S. Logothetidis, L. Viña, and M. Cardona, Phys. Rev. B **31**, 947 (1985).
[58]L. Viña, H. Höchst, and M. Cardona, Phys. Rev. B **31**, 958 (1985).
[59]S. Logothetidis, P. Lautenschlager, and M. Cardona, Phys. Rev. B **33**, 1110 (1985).
[60]S. Logothetidis, M. Cardona, P. Lautenschlager, and M. Garriga, Phys. Rev. B **34**, 2458 (1986).
[61]L. Viña and M. Cardona, Phys. Rev. B **29**, 6739 (1984).
[62]L. Viña and M. Cardona, Phys. Rev. B **34**, 2586 (1986).
[63]L. Viña, C. Umbach, M. Cardona, and L. Vodopyanov, Phys. Rev. B **29**, 6752 (1984).
[64]P. Lautenschlager, S. Logothetidis, L. Viña, and M. Cardona, Phys. Rev. B **32**, 3811 (1985).
[65]P. B. Allen and M. Cardona, Phys. Rev. B **23**, 1495 (1981); **24**, 7479(E) (1981).
[66]P. B. Allen and M. Cardona, Phys. Rev. B **27**, 4760 (1983).
[67]P. Lautenschlager, P. B. Allen, and M. Cardona, Phys. Rev. B **31**, 2163 (1985).
[68]P. Lautenschlager, P. B. Allen, and M. Cardona, Phys. Rev. B **33**, 5501 (1986).
[69]C. K. Kim, P. Lautenschlager, and M. Cardona, Solid State Commun. **59**, 797 (1986).
[70]Y. P. Varshni, Physica (Utrecht) **34**, 149 (1967).
[71]A. Manoogian and J. C. Woolley, Can. J. Phys. **62**, 285 (1984).
[72]U. Fano, Phys. Rev. **124**, 1866 (1961).
[73]G. Abstreiter, M. Cardona, and A. Pinczuk, in *Light Scattering in Solids IV,* edited by M. Cardona and G. Güntherodt (Springer-Verlag, Berlin, 1984), p. 5.
[74]D. E. Aspnes, J. Vac. Sci. Technol. **17**, 1057 (1980).
[75]M. Cardona and H. S. Sommers, Jr., Phys. Rev. **122**, 1382 (1961).
[76]Leitsilber 200, Demetron, Leipzigerstrasse 10, D-6450 Hanau, Federal Republic of Germany.
[77]Ablebond 36-2, Ablestik Laboratories, 833 W. 182nd St., Gardena, CA 90248.
[78]D. E. Aspnes, Opt. Commun. **8**, 222 (1973); D. A. Aspnes and A. A. Studna, Appl. Opt. **14**, 220 (1975), D. E. Aspnes and A. A. Studna, Rev. Sci. Instrum. **49**, 291 (1978).
[79]D. E. Aspnes, J. Opt. Soc. Am. **64**, 812 (1974).
[80]R. M. A. Azzam and N. M. Bashara, *Ellipsometry and Polarized Light* (North-Holland, Amsterdam, 1977).
[81]D. E. Aspnes, G. P. Schwartz, G. J. Gualtieri, A. A. Studna, and B. Schwartz, J. Electrochem. Soc. **128**, 590 (1981).
[82]A. S. Householder, *Principles of Numerical Analysis* (McGraw-Hill, New York, 1953).
[83]A. Savitzky and J. E. Golay, Anal. Chem. **26**, 1627 (1964); J. Steinier, Y. Termonia, and J. Deltour, *ibid.* **44**, 1906 (1972).
[84]Y. Toyozawa, M. Inoue, T. Inui, M. Okazaki, and E. Hanamura, J. Phys. Soc. Jpn. Suppl. **21**, 133 (1966); **22**, 1337

(1967).
[85]J. E. Rowe and D. E. Aspnes, Phys. Rev. Lett. **25**, 162 (1970).
[86]D. E. Aspnes, J. Opt. Soc. Am. **64**, 639 (1974).
[87]G. Dresselhaus, Phys. Rev. **100**, 580 (1955).
[88]E. F. Steigmeier, Appl. Phys. Lett. **3**, 6 (1963).
[89]S. Antoci, E. Reguzzoni, and G. Samoggia, Solid State Commun. **9**, 1081 (1971).
[90]W. Hanke, *Advances in Solid State Physics,* edited by J. Treusch (Vieweg, Braunschweig, 1979), Vol. 19, p. 43.
[91]B. Velicky and J. Sak, Phys. Status Solidi **16**, 147 (1966).
[92]E. O. Kane, Phys. Rev. **180**, 852 (1969).
[93]G. F. Koster and J. C. Slater, Phys. Rev. **96**, 1208 (1954).
[94]R. M. Martin, J. A. Van Vechten, J. E. Rowe, and D. E. Aspnes, Phys. Rev. B **6**, 2500 (1972).
[95]W. Hanke and L. J. Sham, Phys. Rev. B **21**, 4656 (1980).
[96]N. Meskini, W. Hanke, H. J. Mattausch, M. Balkanski, and M. Zouaghi, J. Phys. (Paris) **45**, 1707 (1984).
[97]A. Stahl and I. Balslev, *Electrodynamics of the Semiconductor Band Edge,* in Vol. 110 of *Springer Tracts in Modern Physics* (Springer-Verlag, Berlin, 1987).
[98]A. Stahl, Phys. Status Solidi B **94**, 221 (1979).
[99]A. Stahl, Solid State Commun. **49**, 91 (1984).
[100]I. Balslev, Solid State Commun. **52**, 351 (1984).
[101]M. Cardona, in *Atomic Structure and Properties of Solids,* edited by E. Burstein (Academic, New York, 1972), p. 514.
[102]G. Srinivasan, Phys. Rev. **178**, 1244 (1969).
[103]M. Cardona, in *Light Scattering in Solids II,* edited by M. Cardona and G. Güntherodt (Springer-Verlag, Berlin, 1982), p. 119.
[104]M. Cardona, Phys. Rev. B **15**, 5999 (1977).
[105]A. Daunois and D. E. Aspnes, Phys. Rev. B **18**, 1824 (1978).
[106]D. E. Aspnes and M. Cardona, Solid State Commun. **27**, 397 (1978).
[107]M. Altarelli, Phys. Rev. Lett. **46**, 205 (1981).
[108]P. Lautenschlager, M. Garriga, and M. Cardona (unpublished).